Separation Science and Technology
Publication details, including instructions for authors and subscription information:
http://www.informaworld.com/smpp/title~content=t713708471

Electrical Aspects of Adsorbing Colloid Flotation. XII. Floc Diffusion Rates in Nonideal Systems

R. Moffatt Kennedy III[a]; David J. Wilson[a]
[a] DEPARTMENT OF CHEMISTRY, VANDERBILT UNIVERSITY NASHVILLE, TENNESSEE

To cite this Article Kennedy III, R. Moffatt and Wilson, David J.(1980) 'Electrical Aspects of Adsorbing Colloid Flotation. XII. Floc Diffusion Rates in Nonideal Systems', Separation Science and Technology, 15: 6, 1339 — 1364
To link to this Article: DOI: 10.1080/01496398008068509
URL: http://dx.doi.org/10.1080/01496398008068509

SEPARATION SCIENCE AND TECHNOLOGY, 15(6), pp. 1339–1364, 1980

Electrical Aspects of Adsorbing Colloid Flotation. XII. Floc Diffusion Rates in Nonideal Systems

R. MOFFATT KENNEDY III and DAVID J. WILSON*

DEPARTMENT OF CHEMISTRY
VANDERBILT UNIVERSITY
NASHVILLE, TENNESSEE 37235

Abstract

The dynamics of the diffusion of charged floc particles to charged air–water interfaces is examined within the framework of a modified Gouy-Chapman model in which the finite volumes of floc particles and inert electrolytes were taken into account. The methods of Verwey and Overbeek were used to calculate the electrical free energy of the floc-interface interaction. For the cases considered, diffusion was found to be quite rapid. Fluid mechanical considerations were used to calculate the capture cross-sections of rising bubbles for suspended floc particles; bubbles in the creeping and inviscid flow regimes were considered. These results were used to calculate removal rates from batch and continuous-flow pool-type foam flotation devices.

INTRODUCTION

The applications of foam flotation methods for the removal of inorganics from industrial wastewaters and for the recovery of trace inorganics for analysis have been studied extensively; a number of reviews are available (*1–4*). Grieves, Bhattacharyya, and their co-workers have published extensively on the use of foam flotation techniques in waste treatment; of particular interest to us here are their precipitate flotation studies of chromic hydroxide (*5*) and of wet scrubber wastewaters resulting from SO_2 removal from stack gases (*6*). Their work and the applications of adsorbing colloid flotation to trace metals analyses in seawater by Zeitlin and his co-workers (*7–10*, for example) encouraged us to explore the development of precipitate or adsorbing colloid flotation separations

*To whom correspondence should be addressed.

for a number of inorganic contaminants in industrial wastewaters (*11–15*). We also investigated the theory of the adsorption of precipitates at the air–water interface (*16–19*); Huang and Lee have also published recently on the coulombic model for precipitate–bubble attachment (*20*).

One of the problems of interest in the flotation of flocs and precipitates is the dynamics of the forced diffusion of the particles to the air–water interface. The rate of this process, the range of the attractive force, the pattern of the streamlines of the liquid relative to the rising bubble, and the rise velocity of the bubble determine the efficiency of the bubble in scavenging the particles from the solution. Huang used a simplified Gouy-Chapman model previously to examine forced diffusion of particles to the air–water interface (*21*); we here investigate a more exact model in which the attractive force is calculated by a modification of the method of Verwey and Overbeek for calculating the free energy of interaction (*22*) which takes into account the finite volumes of the ions (*16*). This yields information about the distance from which a bubble may attract a floc particle as liquid streams pass the rising bubble. We then examine the streamlines of the liquid flowing past the bubble to determine the effective collision cross-section of the bubble for floc particles. With this result it becomes possible for us to calculate rates of floc removal from both dilute and concentrated suspensions in batch and continuous-flow pool flotation experiments.

NONIDEAL DIFFUSION

Analysis

We examine the diffusion of charged particles in a thin film of water bounded by two air–water interfaces onto which a charged surfactant is absorbed. We let

L = the distance between the two air–water interfaces
ψ_0 = surface potential of the air–water interfaces
ψ_1 = surface potential of the floc due to its adsorption of potential-determining ions
x = distance from the left air–water interface

See Fig. 1. When the floc is of opposite potential to the air–water interface, the electrical attraction between this interface and the particles causes a migration of particles until the increase in particle chemical potential due to increased particle concentration balances out the decrease in the electrical potential energy of the particle. The solution is divided into $2N$ slabs of unit area oriented parallel to the air–water interfaces. The distance of

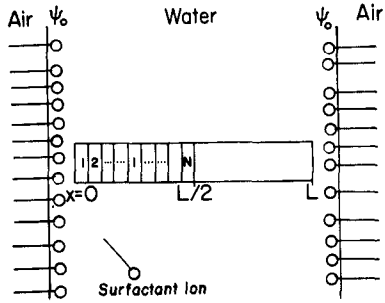

FIG. 1. The model for analysis of diffusion rates in films.

closest approach of a particle to the surface is considered to be 10 Å. Note that there is no net diffusion across the center of the film due to the symmetry of the problem, so that we need deal with only that half of the solution between 0 and $L/2$.

The electrical potential in the region between the air–water interface and the water–floc interface is calculated by the method used previously (*23*), as outlined below. A 1–1 electrolyte is assumed, the ions of which are of comparable radius. The chemical potential is taken to be

$$\mu^{\pm}(x) = \mu_0{}^{\pm} \pm e\psi(x) + KT \ln c^{\pm}(x) + kT \ln \frac{c_{max}}{c_{max} - (c^{+} + c^{-})} \quad (1)$$

where $\mu^{\pm}$ = chemical potential of cation (anion)
$c^{\pm}$ = cation (anion) concentration, ions/cm^3
c_{max} = maximum electrolyte ion concentration

The last term corrects for the nonideality of the inert electrolyte due to the finite volumes of the ions. At large distances from the surface the electric potential decreases to zero so that

$$\mu^{\pm}(\infty) = \mu_0{}^{\pm} + kT \ln c_{\infty} + kT \ln \frac{c_{max}}{c_{max} - 2c_{\infty}} \quad (2)$$

where c_{∞} is the salt concentration in the bulk solution. Since the chemical potentials at equilibrium are independent of x, they may be equated, yielding

$$\ln c_{\infty} + \ln \frac{c_{max}}{c_{m}{}^{e}{}_{x} - 2c_{\infty}} = \pm \frac{e\psi(x)}{kT} + \ln c^{\pm}(x) + \ln \frac{c_{max}}{c_{max} - [c^{+}(x) - c^{-}(x)]} \quad (3)$$

Now let

$$f^{\pm} = \frac{c^{\pm}}{c_{max} - (c^{+} + c^{-})} = \frac{c_{\infty}}{c_{max} - 2c_{\infty}} \exp\left(\mp \frac{e\psi(x)}{kT}\right) \tag{4}$$

from which we find

$$c^{\pm}(x) = \frac{c_{max} f^{\pm}}{1 + f^{+} + f^{-}} \tag{5}$$

The charge density in solution is given by

$$\rho = e(c^{+} - c^{-}) \tag{6}$$

Substitution of Eqs. (4) and (5) into (6), and (6) into Poisson's equation yields the modified Poisson-Boltzmann equation

$$\frac{d^2\psi}{dx^2} = \frac{A \sinh(e\psi/kT)}{1 + B \cosh(e\psi/kT)} \tag{7}$$

where

$$A = \frac{8\pi e c_{\infty}}{(1 - 2c_{\infty}/c_{max})D}$$

and

$$B = 2c_{\infty}/(c_{max} - 2c_{\infty})$$

For ions of |charge| *ve*, replace *e* by *ve* in these equations. Verwey and Overbeek present a complete discussion of the ideal case (*22*).

The free energy of interaction per unit area between the fixed potential surfaces is calculated by a method discussed by Devereux and deBruyn (*24*). The charges of all ions, those adsorbed and those in solution, are imagined to be gradually built up in infinitesimal steps, *ve* $d\lambda$. Lambda, λ, the charging parameter, varies from 0 to 1, and *v* is the valence of the ions. The free energy is equivalent to the work required to charge the double layers reversibly and isothermally plus a term contributed when $\lambda = 0$. The equilibrium condition for adsorption is

$$\Delta\mu + ve\psi_0 = 0 \tag{8}$$

where $\Delta\mu$ is the difference of the chemical potentials of an adsorbed ion and a free ion in solution, and ψ_0 is the surface potential of the air–water interface. In charging the adsorbed layer, the chemical potential difference, $\Delta\mu$, is considered to vary also; otherwise, as λ approaches zero, the surface potential is forced to infinity:

$$\Delta\mu + \lambda ve\psi_0 = 0 \tag{9}$$

Therefore

$$\lambda\Delta\mu + \lambda ve\psi_0 = 0 \tag{10}$$

and ψ_0 remains constant. This condition has the advantage that the electrical work done in charging the adsorbed ions is exactly canceled by the change in chemical free energy of adsorption. The total free energy of the double layer is thus determined by the electrical work required to charge the ions in solution. The argument is exactly analogous for ψ_1, the water–floc surface potential. The charge density and potential at a point in solution for a particular value of λ we take as ρ' and ψ', respectively. The net excess concentration of charge determining ions is then $\rho'/\lambda ve$, and the work required to increase the charge of these ions by $ve\, d\lambda$ is $\rho'\psi'\, d\lambda/\lambda$. This work differential is integrated over the volume of solution to complete charge:

$$G_s = \int_0^1 \frac{d\lambda}{\lambda} \iiint \psi'\rho'\, dx\, dy\, dz \tag{11}$$

Since ψ_0 and ψ_1 are constant, the double layers will have a nonzero potential energy at $\lambda = 0$, which is dependent upon the distance separating the two planes, d. For parallel planes,

$$G(0) = \frac{D}{8\pi d}(\Delta\psi)^2 \tag{12}$$

where

$$\Delta\psi = \psi_1 - \psi_0$$

The total energy for the system is therefore expressed by

$$G(d) = -\frac{D}{8\pi d}(\Delta\psi)^2 + \int_0^1 \frac{d\lambda}{\lambda} \iiint \psi'\rho'\, dx\, dy\, dz \tag{13}$$

The analysis (*23*) is outlined as follows. For the geometry of the system being considered, parallel planes, the space integration simplifies to one variable, x. The surface potentials may also be substituted, giving

$$G(d) = -\frac{D}{8\pi d}(\psi_1 - \psi_0)^2 + \int_0^1 \int_0^d \frac{\rho'\psi'}{\lambda}\, dx\, d\lambda \tag{14}$$

Poisson's equation and Eq. (7) give

$$\rho' = \frac{D}{4\pi}\frac{\partial^2\psi'}{\partial_x 2} = -\frac{D}{4\pi}\frac{\lambda A \sinh(\beta e\lambda\psi)}{1 + B\cosh(\beta e\lambda\psi)} \tag{15}$$

where

$$\beta = 1/kT$$

Substituting Eq. (15) and the identity

$$\psi' \, d\lambda = \frac{\partial}{\partial \lambda}(\lambda\psi') \, d\lambda - \frac{\partial \psi'}{\partial \lambda} \, d\lambda \tag{16}$$

into Eq. (14) yields

$$\begin{aligned} G(d) &= -\frac{D}{8\pi d}(\psi_1 - \psi_0)^2 - \int_0^d \int_0^1 \frac{DA \sinh(\beta e \lambda \psi')}{4\pi[1 + B\cosh(\beta e \lambda \psi')]} \frac{\partial}{\partial \lambda}(\lambda\psi') \, d\lambda \, dx \\ &\quad + \int_0^d \int_0^1 \frac{D}{4\pi} \frac{\partial \psi'}{\partial \lambda} \frac{\partial^2 \psi'}{\partial x^2} \, d\lambda \, dx \\ &= -\frac{D}{8\pi d}(\psi_1 - \psi_0)^2 + I_1 + I_2 \end{aligned} \tag{17}$$

Integrating I_1 with respect to $(\lambda\psi')$ gives

$$I_1 = -\int_0^d \frac{DA}{4\pi e \beta B} \ln\left[\frac{1 + B\cosh(\beta e \psi)}{1 + B}\right] dx \tag{18}$$

As has been shown (*24*),

$$I_2 = -\frac{D}{8\pi} \int_0^d \int_0^1 \frac{\partial}{\partial \lambda}\left(\frac{\partial \psi'}{\partial x}\right)^2 d\lambda \, dx \tag{19}$$

which integrates to

$$I_2 = -\frac{D}{8\pi} \int_0^d \left(\frac{\partial \psi}{\partial x}\right)^2 dx + \frac{D}{8\pi d}(\psi_1 - \psi_0)^2 \tag{20}$$

In order to change the variable of integration, the first integral of Eq. (7) is obtained by Newton's method:

$$\frac{d\psi}{dx} = \left[\left.\frac{d\psi}{dx}^2\right|_{x=0} + \frac{2A}{e\beta B} \ln \frac{1 + B\cosh(e\beta\psi)}{1 + B\cosh(e\beta\psi_0)}\right]^{1/2} \tag{21}$$

Equations (20) and (18) are now substituted into Eq. (17), changing the variable of integration from x to ψ, to obtain

$$G(d) = -\frac{D}{8\pi} \int_{\psi_0}^{\psi_1} \frac{H + c \ln \dfrac{(1 + B\cosh\beta e\psi)^2}{(1 + B)(1 + B\cosh\beta e\psi_0)}}{\left[H + c \ln \dfrac{1 + B\cosh\beta e\psi}{1 + B\cosh\beta e\psi_0}\right]^{1/2}} d\psi \tag{22}$$

where

$$H = \left.\left(\frac{d\psi}{dx}\right)^2\right|_{x=0} \quad \text{and} \quad c = \frac{2A}{e\beta B} \tag{23}$$

At infinite separations, $G(\infty)$ is not zero, due to the existence of double

layers at each interface. Since the free energy of interaction of the double layers is the quantity desired, $G(d)$ must be referenced to $G(\infty)$. $G(\infty)$ is calculated as follows. From Eq. (21),

$$x(\psi) = \int_{\psi_0}^{\psi} \frac{d\psi^*}{\left[H + c \ln \dfrac{1 + B \cosh \beta e \psi^*}{1 + B \cosh \beta e \psi_0}\right]^{1/2}} \tag{23a}$$

Now if $d \to \infty$, the denominator of the integrand must vanish as $\psi \to 0$ since the limits of the integral are finite. Therefore

$$H\Big|_{\substack{x=0 \\ d=\infty}} = H(\infty) = c \ln \frac{1 + B \cosh \beta e \psi_0}{1 + B} \tag{24}$$

so that

$$G(\infty) = -\frac{D}{8\pi} \int_{\psi_0}^{\psi} \frac{H(\infty) + c \ln \dfrac{(1 + B \cosh \beta e \psi)^2}{(1 + B)(1 + B \cosh \beta e \psi_0)}}{\left[H(\infty) + c \ln \dfrac{1 + B \cosh \beta e \psi}{1 + B \cosh \beta e \psi_0}\right]^{1/2}} \tag{25}$$

The following usage of G is with respect to $G(\infty)$, i.e.,

$$G = G(d) - G(\infty)$$

The chemical potential of a floc particle we take as given as a function of position by

$$\mu(x) = \mu_0 + G(x) + kT \ln \left[C \frac{1}{1 - C/C_M}\right] \tag{26}$$

The activity coefficient, $(1 - C/C_M)^{-1}$, which is analogous to the one used previously for the electrolyte, corrects for the excluded volume of the floc particles; C is the concentration of floc particles which is understood to be a function of two variables, x and time t.

The differential equation governing isothermal diffusion in a fluid medium in the presence of a varying chemical potential is

$$\frac{\partial C}{\partial t} = \frac{1}{6\pi\eta r_0} \nabla(C \nabla \mu) \tag{27}$$

where η is the fluid viscosity and r_0 is the effective radius of the particle. In planar geometry, Eq. (27) simplifies to

$$\frac{\partial C}{\partial t} = \frac{1}{6\pi\eta r_0} \frac{\partial}{\partial x}\left(C \frac{\partial \mu}{\partial x}\right) \tag{28}$$

Substitution of Eq. (26) into Eq. (28) yields a nonlinear partial differential equation which is not solvable in closed form. In addition, values of $G(x)$

are not given in a closed form. Therefore it is necessary to integrate the equation numerically. A predictor-corrector method (*25*) was utilized which has been shown to have good stability (*21*) in problems of this type. From Fick's First Law of Diffusion we see that the term in parenthesis in Eq. (28) is proportional to the negative flux of particles at a point in the solution. For the cell model being considered, the flux at the right-hand side, the side toward the bulk solution, of the ith cell is taken to be

$$J_i^{\text{OUT}} = -\left(\frac{C_{i-1} + C_i}{2}\right)\frac{\partial \mu_{i-1}}{\partial x}\frac{1}{6\pi\eta r_0} \tag{29}$$

The superscript "OUT" indicates that the migration of particles is out of the cell if $\partial\mu_i/\partial x$ is positive and the average of the concentrations approximates that at the wall. The flux into the cell at the left-hand wall (if $\partial\mu_{i-1}/\partial x$ is positive) is

$$J_i^{\text{IN}} = -\left(\frac{C_{i-1} + C_i}{2}\right)\frac{\partial \mu_{i-1}}{\partial x}\frac{1}{6\pi\eta r_0} \tag{30}$$

The finite difference representation of Eq. (28) for the change with time in the number of particles in the ith cell is

$$\frac{\partial C_i(t)}{\partial t} = \frac{1}{\Delta x}(J_i^{\text{IN}} - J_i^{\text{OUT}}) \tag{31}$$

Substituting Eqs. (29) and (30) into Eq. (31) and including the finite difference representation of the derivatives of the potentials gives the final form

$$\frac{\partial C_i(t)}{\partial t} = \frac{1}{6\pi\eta r_0}\frac{1}{\Delta x}\left[\left(\frac{C_{i+1} + C_i}{2}\right)\left(\frac{\mu_{i+1} - \mu_i}{\Delta x}\right) - \left(\frac{C_{i-1} + C_i}{2}\right)\left(\frac{\mu_i - \mu_{i-1}}{\Delta x}\right)\right] \tag{32}$$

Let

$$\frac{\partial C_i(t)}{\partial t} = f(\mu_{i+1}, \mu_i, \mu_{i-1}, C_{i+1}, C_i, C_{i-1}) \tag{33}$$

Equations (33) are now integrated with respect to t by the predictor-corrector method.

Predictor:

$$\bar{C}_i(t + \Delta t) = C_i(t - \Delta t) + 2\Delta t\frac{\partial C_i(t)}{\partial t} \tag{34}$$

$$\frac{\partial \bar{C}_i(t + \Delta t)}{\partial t} = f[\bar{\mu}_{i+1}(t + \Delta t), \bar{\mu}_i(t + \Delta t), \bar{\mu}_{i-1}(t + \Delta t), \bar{C}_{i+1}, \bar{C}_i, \bar{C}_{i-1}] \tag{35}$$

Corrector:

$$C_i(t + \Delta t) = C_i(t) + \frac{\Delta t}{2}\left[\frac{\partial C_i(t)}{\partial t} + \frac{\partial \bar{C}_i(t + \Delta t)}{\partial t}\right] \tag{36}$$

The starter formula for the use of the predictor-corrector is taken from Euler's method:

$$C_i(t + \Delta t) = C_i(t) + \Delta t \frac{\partial C_i(t)}{\partial t} \tag{37}$$

The boundary conditions are given by the requirements that there be no flux of floc particles at $x = 0$ and $x \doteq L/2$, the center of the aqueous film. Then, in the first cell,

$$J_1^{\text{IN}} = 0$$

which gives

$$\frac{\partial C_i(t)}{\partial t} = \frac{1}{6\pi\eta r_0}\frac{1}{\Delta x}\left[\left(\frac{C_2 + C_1}{2}\right)\left(\frac{\mu_2 - \mu_1}{x}\right)\right] \tag{38}$$

In the Nth cell,

$$J_N^{\text{OUT}} = 0$$

Therefore

$$\frac{\partial C_N(t)}{\partial t} = \frac{1}{6\pi\eta r_0}\frac{1}{\Delta x}\left[-\left(\frac{C_{N-1} + C_N}{2}\right)\left(\frac{\mu_N - \mu_{N-1}}{\Delta x}\right)\right. \tag{39}$$

A necessary condition of the numerical representation is that it conserves the total number of particles in the film at all times; i.e.,

$$\int_0^{L/2} \frac{\partial C(x, t)}{\partial t}\, dx = \sum_{i=1}^{N} \frac{\partial C_i(t)\Delta x}{\partial t} = 0, \qquad \text{for all } t \tag{40}$$

This requirement may be seen to be fulfilled by summing Eq. (31), noting that $J_{i+1}^{\text{IN}} = J_j^{\text{OUT}}$ and that $J_i^{\text{IN}} = J_N^{\text{OUT}} = 0$.

The concentration profile at equilibrium may be calculated by equating the chemical potentials of the floc particles in the potential field and in the bulk solution, where $G(\infty) = 0$. This gives

$$G_i + kT \ln \frac{C_i^e}{1 - C_i^e/CM} = kT \ln \frac{C_\infty}{1 - C_\infty/C_M} \tag{41}$$

which yields

$$C_i^e = \frac{C_\infty \exp(-G_i/kT)}{1 + C_\infty/C_M[\exp(-G_i/kT) - 1]} \tag{42}$$

To estimate the rate at which a nonequilibrium initial distribution of particles approaches the final equilibrium distribution, the following function is computed:

$$V(t) = \sum_{i=1}^{N} [C_i(t) - C_i^e]^2 \Big/ \sum_{i=1}^{N} C_i^2(0) \tag{43}$$

$V(t)$ is the statistical variance of the concentration from that at equilibrium, divided by a normalizing factor. In all of the following calculations this initial distribution was taken as constant throughout the film and of a value of 10^{-4} C_M, except where noted. A semilog plot of $V(t)$ vs t will yield information on the nature of the decay to equilibrium. Where essentially linear plots are obtained, the decay to equilibrium is exponential. The slope is then twice the rate constant, k, due to squaring the differences in $V(t)$. The range over which the rate constant varies may be deduced if the plot is appreciably nonlinear.

Results

Concentration distributions of floc particles at various times are shown in Fig. 2 for a 100-Å film. Since they are symmetrical, the curves are drawn only to $L/2$. The closest approach of the colloid to the air–water interface is restricted to 10 Å. The parameters of the system are given in the caption. In all calculations the values of the dielectric constant and viscosity of the solvent were taken as those at 25°C, viz., 78.54 and 0.01 poise, respectively, except where influence of these parameters was investigated. The floc radius was 5.64 Å. It can be seen that there is initially a rapid influx of particles in the region nearest the charged surface. Minima in the curves are seen to develop since thermal diffusion is not fast enough to fill the depleted area. These regions progress into the solution until at equilibrium the curve is monotonic, the minimum occurring in the center of the film. The slopes of these curves should be zero at $L/2$ since $\partial\mu/\partial x = 0$ at that point. In fact, $\partial\mu/\partial x$ is not zero there for this 100 Å film; at $x = L/2$ the particle still has a nonzero interaction energy with the air–water interface which is at $x = 0$, and the influence of the other air–water interface at $x = L$ is neglected in our calculation. Figure 3 shows similar plots for a 200-Å film in which $\partial C/\partial x$ is essentially zero at $x = L/2$. There is no interaction at that distance, $\psi(L/2) \cong 0$, so that $\partial\mu/\partial x \cong 0$ in the center. This

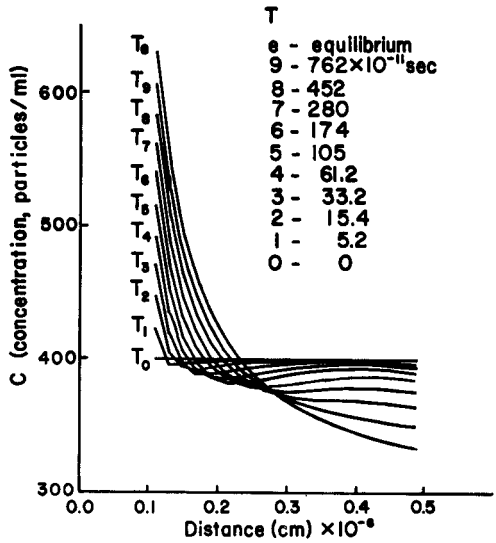

FIG. 2. Colloid concentration vs distance from the air–water interface at various times, $L = 100$ Å. $\psi_0 = -50$ mV, $\psi_1 = 50$ mV, $c_{max} = 10^{-2}$ mole/cc, $c_\infty = 10^{-5}$ mole/cc.

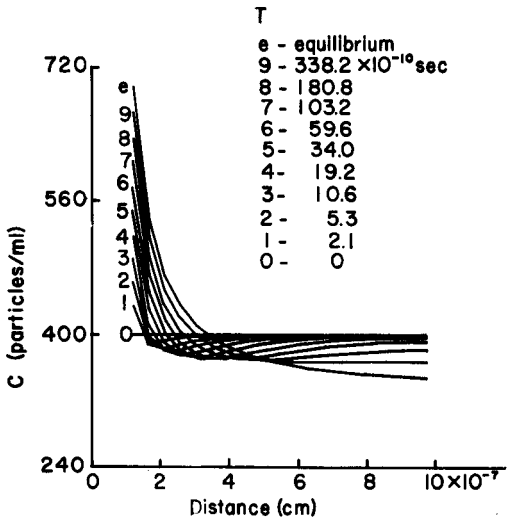

FIG. 3. Colloid concentration vs distance from the air–water interface at various times, $L = 200$ Å. $\psi_0 = -50$ mV, $\psi_1 = 50$ mV, $c_{max} = 10^{-3}$ mole/cc, $c_\infty = 10^{-5}$ mole/cc.

problem is not a factor in the calculations of the rate constants, since this 200 Å film is the thinnest we normally considered.

Figure 4 shows the time dependence of $V(t)$ at various inert 1–1 electrolyte concentrations. After initial rapid decay, the slope of ln $V(t)$ vs t becomes constant for these 400 Å films. Rate constants for these curves are given in Table 1. Also in Table 1 are the rate constants calculated with other values of c_{max}. For $c_{max} = 10^{-2}$ mole/cc, increasing the electrolyte concentration from 10^{-5} to 10^{-3} mole/cc increases the rate constant, and in the range of 10^{-5} to 10^{-7} mole/cc the rate constant varies negligibly. In the latter range the free energy of interaction is large near the air–water interface and extends a great distance into the film. This condition necessitates large changes in the floc concentrations as equilibrium is approached; positive near $x = 0$ and negative near $x = L/2$. Therefore a large fraction of the total number of particles must migrate from the bulk solution to the surface. After initial redistribution due to electrical forces, migration is increasingly due simply to random movement. Therefore the rate constants are smaller than those in the $c_\infty = 10^{-5}$ to 10^{-3} mole/cc range. In this more concentrated range the free energy near the surface is rapidly decreasing in absolute value with increasing salt concentration,

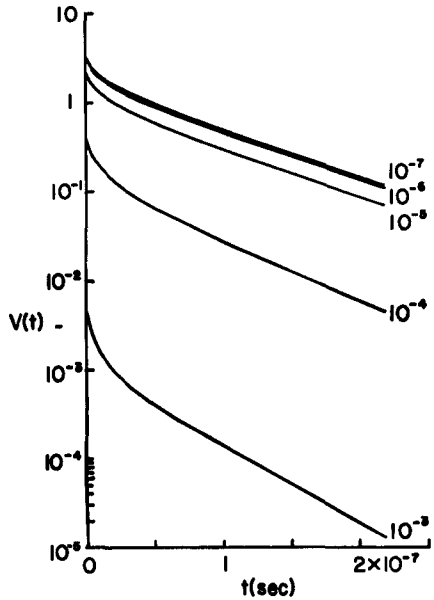

FIG. 4. Change of $V(t)$ with time at several inert electrolyte concentrations (given beside each curve in mole/cc). $c_{max} = 10^{-2}$ mole/cc, $\psi_0 = -100$ mV, $\psi_1 = 100$ mV, $L = 400$ Å.

TABLE 1

Variation of Rate Constants with Inert Salt Concentration[a]

c_{max} (mole/cc)	c (mole/cc)	$k \times 10^{-6}$ (sec^{-1})
10^{-4}	10^{-5}	5.908
	10^{-6}	6.006
	10^{-7}	6.071
10^{-3}	10^{-4}	7.152
	10^{-5}	5.975
	10^{-6}	6.002
	10^{-7}	6.072
10^{-2}	10^{-3}	10.063
	10^{-4}	7.618
	10^{-5}	5.993
	10^{-6}	6.001
	10^{-7}	6.072

[a]Conditions: $L = 400$ Å, $\psi_0 = -100$ mV, $\psi_1 = 100$ mV.

while at the same time the extent to which the potential's influence reaches out into the solution decreases due to ionic screening. The resulting decrease in equilibrium particle concentration in the vicinity of the air–water interface causes an increase in the rate constant since the transfer of particles from one region of the film to another is not so extensive. The effect of nonideality of the salt is small, but may be seen by examining data at $c_\infty = 10^{-5}$ mole/cc, at which the rate constant is seen to decrease with decreasing maximum concentration, c_{max}. These rate constants may be compared to the eigenvalues obtained in the simple one-dimensional diffusion problem with absorbing boundaries, the lowest of which is

$$\lambda_d = \frac{\pi kT}{6\eta r_0 L^2} \tag{44}$$

For the conditions in Table 1, $\lambda_d = 2.4 \times 10^6$ sec^{-1}. This least value is not a close approximation to the driven diffusion rate constants.

The effects of varying the electric potentials are next examined. Figure 5 shows the change of $V(t)$ with ψ_1, the water–floc potential, and Table 2 gives the rate constants. As ψ_1 decreases, the rate constant increases. The explanation is the same as the one for the case of salt concentration dependence; increasing the potential increases the amount of colloid that must migrate past a given plane. After a quick redistribution in the electric field, migration is limited by thermal diffusion. The effects are reciprocal in that interchanging the absolute values of ψ_0 and ψ_1 does not change the rate constant since the potential energy is unchanged; this gives a consistency check on our analysis and computer programs.

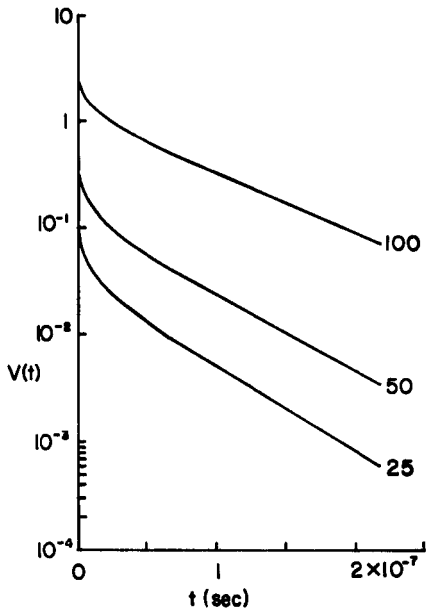

FIG. 5. Change of $V(t)$ with time at several water–floc potentials (ψ_1 given beside each curve in mV). $\psi_0 = -100$ mV, $c_{max} = 10^{-2}$ mole/cc, $c = 10^{-5}$ mole/cc, $L = 400$ Å.

TABLE 2

Variation of Rate Constants with the Surface Potentials[a]

ψ_0 (mV)	ψ_1 (mV)	$k \times 10^{-6}$ (sec^{-1})
−100	100	5.966
−100	50	7.912
−100	25	8.876
−50	100	7.912
−50	50	9.358
−50	25	9.903
−25	100	8.876
−25	50	9.903
−25	25	10.22

[a]Conditions: $c_{max} = 10^{-2}$ mole/cc, $c = 10^{-5}$ mole/cc, $L = 400$ Å.

Rate constants increase with increasing temperature as shown in Table 3. In Table 4 is the variation in rate with the radius of the floc particle. Increasing the radius decreases the rate constant. Evidently the effect of the increased viscous drag, which affects particle motions throughout the

TABLE 3

Variation of Rate Constants with Temperature

Temperature (°C)	$k \times 10^{-6}$ (sec^{-1})
10	8.739
25	9.358
50	10.38
75	11.39
90	11.97

TABLE 4

Variation of Rate Constants with Floc Radius[a]

Radius (Å)	$k \times 10^{-6}$ (sec^{-1})
5.64	9.358
6.77	7.358
7.90	5.870
9.03	4.731
10.14	3.824
11.28	3.129
14.10	2.074
16.93	1.652

[a]Conditions: $L = 400$ Å, $c_{max} = 10^{-2}$ mole/cc, $c = 10^{-5}$ mole/cc, $\psi_0 = -50$ mV, $\psi_1 = 50$ mV.

TABLE 5

Variation of Rate Constants with Electrolyte Charge

Charge (elementary units of charge)	$k \times 10^{-6}$ (sec^{-1})
1	9.358
2	9.686
3	10.05

solution, is greater than that of the increased electrostatic attraction, which operates only in the boundary layer where an electric potential gradient exists.

In Table 5, rate constants are seen to increase with increasing charge of the 1–1 electrolyte. The explanation is as before when the electric potential is changed by screening due to increased electrolyte concentration; a smaller amount of floc must be moved. The small variation of the rate constants with initial floc concentration, shown in Table 6, indicates the excluded volume of the particles has only a minor effect. The initial concentrations are fractions of the maximum floc concentration, C_M. Rate

TABLE 6

Variation of Rate Constants with Initial Floc Concentration[a]

Initial concentration (mole/cc)	$k \times 10^{-6}$ (sec^{-1})
$10^{-4}\ C_M$	9.368
$10^{-3}\ C_M$	9.368
$10^{-2}\ C_M$	9.482
$10^{-1}\ C_M$	10.69

[a]Conditions: $L = 400$ Å, $c_{max} = 10^{-2}$ mole/cc, $c = 10^{-5}$ mole/cc, $\psi_0 = -50$ mV, $\psi_1 = 50$ mV.

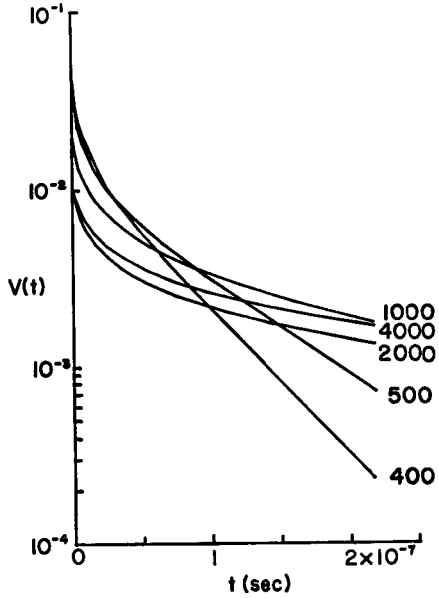

FIG. 6. Change of $V(t)$ with time at several film lengths (L given beside each curve in Å). $\psi_0 = -50$ mV, $\psi_1 = 50$ mV, $c_{max} = 10^{-2}$ mole/cc, $c = 10^{-5}$ mole/cc.

constants increase with increasing concentration, which is probably due to a limitation of the total movement of particles when concentrations in the vicinity of the air–water interface are near the maximum possible.

The last plot shows changes in $V(t)$ at film thicknesses of 400 to 4000 Å. The data in Fig. 6 yield the rate constants in Table 7. As expected from Eq. (44), the rate constants decrease with increasing thickness of the film. The decrease approximates the inverse square relationship for very thin

TABLE 7

Variation of Rate Constants with Film Length

Length (Å)	$k \times 10^{-6}$ (sec^{-1})
200	41.90
400	9.358
500	5.598
750	2.957
1000	2.172
2000	1.554
3000	1.442
4000	1.381

TABLE 8

Change of the Rate Constant with Time for $L = 4000$ Å[a]

Time $\times 10^7$ (sec)	$k \times 10^{-6}$ (sec^{-1})
2.19	1.381
8.72	0.414
34.8	0.139

[a]Conditions: $\psi_0 = -50$ mV, $\psi_1 = 50$ mV, $c_{max} = 10^{-2}$ mole/cc, $c = 10^{-5}$ mole/cc.

films but does not adhere at all to that relationship for thicker films. Close examination of the graphs shows $V(t)$ not to be linear at longer lengths, however, and indeed, Table 8 shows a dramatic change in k with time. Calculation of k at the longest time required 5 min of computer time; therefore, to search for a limiting value of k would require excessive computer time. It is concluded then that for a large film thickness, k varies over a wide range of values, though still large, and does not soon become constant as was thought in the ideal case (*21*). Most of the rate constants determined in this nonideal case are slightly less than those calculated by the ideal model. Since the parameter values of the ideal and nonideal models were not exactly the same, an exact comparison is not possible, but values in this work may be extrapolated to the conditions of the ideal case. Interpolating between $L = 200$ Å and $L = 400$ Å to the value of 300 Å used in the ideal model and also to a particle radius of 10 Å gives a rate constant of 6×10^6 sec^{-1}. The range reported in the ideal case was 1.5 to 2.0 $\times 10^7$ sec^{-1}.

Conclusions

The nonideal model, which includes activity coefficients for the chemical potentials of the colloid and inert electrolyte and improved calculation of

interaction potentials, gives rate constants typically one-third to one-half those of the ideal model. These values, of the order of 6×10^6 sec^{-1}, are exceedingly large, so that the particle distribution near interfaces in a dynamic system, such as a flotation cell, must approach that at equilibrium. This equilibrium may be shifted to a higher density of colloid in the air–water surface region (thus increasing separation efficiency) by increasing one or both of the surface potentials, air–water or water–floc, decreasing dissolved electrolytes, or increasing particle area, but associated with these changes is a decrease in the rate of approach to that equilibrium. This result is apparently due to the increase in the total movement of the particles in the film. The approach to equilibrium does not become an exponential decay for films greater than 1000 Å until extremely long times have elapsed.

FLUID MECHANICS OF FLOC–BUBBLE ATTACHMENT

Here we examine the rate at which a bubble rising through a pool of liquid encounters and captures floc particles in its path. We consider that the liquid is at rest except for the disturbance of the rising spherical bubble which is moving at a terminal velocity determined by its buoyancy and viscous drag. In order for capture to occur, we assume that the surface of the bubble must pass within a distance δ of the floc particle, and we assume that the floc particles as seen from the bubble move past it on the streamlines of the liquid as the bubble rises.

The Reynolds number for a sphere moving in a fluid is

$$\mathrm{Re} = 2av\rho/\eta \tag{45}$$

where a = sphere radius
v = sphere velocity
ρ = liquid density
η = liquid viscosity

For $\mathrm{Re} \leq 10^4$, it can be shown that (*26*)

$$v = \frac{2g\rho a^2}{9\eta}\left[1 + \frac{1}{4}\left(\frac{\rho av}{2\eta}\right)^{1/2} + \frac{0.34\rho av}{12\eta}\right]^{-1} \tag{46}$$

For $\mathrm{Re} < 1$, Stokes' law holds pretty well; one has viscous, streamlined flow past the sphere, and no eddy wake is formed. At larger Reynolds numbers a turbulent wake is formed, viscous forces become small compared to momentum forces, and we can approximate the flow as inviscid (*27*). The maximum bubble size for which we have viscous, creeping flow is given by setting $\mathrm{Re} = 1$ and equating the buoyancy force and the

Stokes' law viscous drag force

$$\frac{4\pi}{3}\rho a^3 g = 6\pi\eta a v \tag{47}$$

These relationships yield

$$a = \left(\frac{9\eta^2}{4\rho^2 g}\right)^{1/3} = 6.12 \times 10^{-3}\ \text{cm} \tag{48}$$

for water.

We next examine the path of elements of a viscous fluid in creeping flow around a rising bubble. The streamlines can be written as

$$z = \left(2y^2 - 3y + \frac{1}{y}\right)\sin^2\theta \tag{49}$$

The situation is diagrammed in Fig. 7. Here $y = r/a$, and for any particular streamline z = a constant. For points a great distance in front of or behind the bubble (ρ finite, $|x| \to \infty$), we have

$$z = 2y^2 \sin^2\theta = \frac{2r^2}{a^2}\frac{\rho_\infty{}^2}{r^2} = \frac{2\rho_\infty{}^2}{a^2} \tag{50}$$

The streamlines (plotted in Fig. 8) come closest to the bubble when $\theta = \pi/2$, since

$$\frac{dy}{d\theta} = -\frac{(4y^4 - 3y^3 + y)}{4y^3 - 3y^2 - 1}\cot\theta = 0, \qquad \text{when } \theta = \pi/2 \tag{51}$$

For $\theta = \pi/2$ we have

$$\frac{2\rho_\infty^2}{a^2} = \left(2y^3 - 3y + \frac{1}{y}\right) \tag{52}$$

We let $r = a + \delta$, where δ is the distance across which coulombic attraction could pull the particle to the bubble surface in the time available. So $y = 1 + \delta/a$, and we assume that $\delta/a \ll 1$. Substitution of this expression

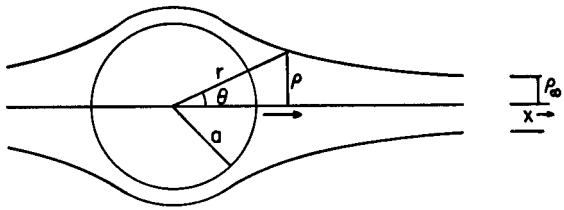

FIG. 7. A bubble rising through a liquid—notation.

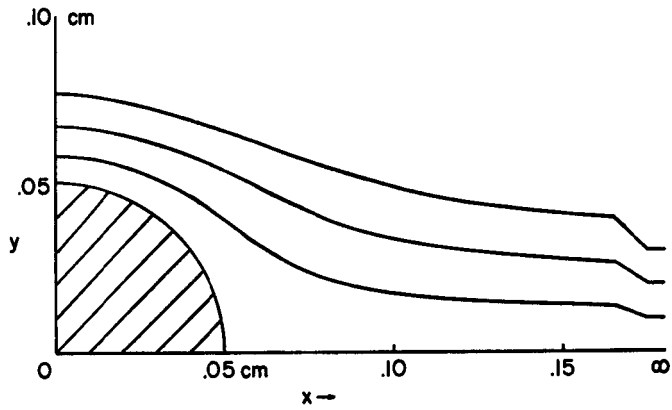

FIG. 8. Streamlines about a bubble rising through a liquid in the creeping flow regime.

for y into Eq. (52) and expansion of $1/y$ in ascending powers of δ/a then yields

$$\frac{2\rho_\infty{}^2}{a^2} = 3(\delta/a)^2 \tag{53}$$

so that

$$\rho_\infty \leqq \sqrt{3/2}\delta \tag{54}$$

if the particle is to be captured as the bubble passes. A particle must lie within a distance $\sqrt{3/2}\delta$ of the path of the center of the bubble in order for it to be able to attach to the bubble as it passes. Since the range of the particle–bubble forces is rather short, we see that the actual volume of liquid from which particles would be swept as the bubble rises a distance h is quite small, given by

$$V_{cf} = \pi\rho_\infty{}^2 h = (3/2)\pi\delta^2 h \tag{55}$$

The above analysis is based on the assumption that the bubbles are small enough to be in the viscous creeping flow regime. If the bubbles are larger, inertial effects become more important, and we approach the case of inviscid flow. We next examine this case, but must neglect the turbulence in the wake of the bubble—we assume an ideal inviscid liquid. For this case the streamlines are given by (*27*)

$$z = \left(2y^2 - \frac{2}{y}\right)\sin^2\theta \tag{56}$$

where our notation is as before. It is readily shown that z is again given by

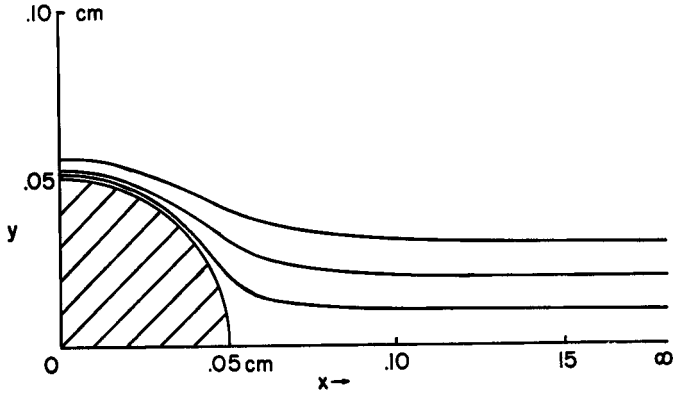

FIG. 9. Streamlines about a bubble rising through a liquid in the inviscid flow regime.

Eq. (50), and that the streamlines approach most closely to the bubble when $\theta = \pi/2$. See Fig. 9. We again let $y = 1 + \delta/a$, substitute into Eq. (56), expand $1/y$ in ascending powers of δ/a, and truncate the series to obtain

$$\frac{2\rho_\infty{}^2}{a^2} = 6\frac{\delta}{a} + 0\left(\frac{\delta}{a}\right)^2 + \cdots \tag{57}$$

so that

$$\rho_\infty = \sqrt{3\delta a} \tag{58}$$

if a particle is to be captured. The volume of liquid from which particles are captured when the bubble rises a distance h is

$$V_{if} = \pi\rho_\infty{}^2 h = 3\pi\delta a h \tag{59}$$

which is very much larger than the corresponding volume for the case of creeping flow, given by Eq. (55).

We next calculate the rate of removal of floc particles by flotation from a column of liquid of height h through which bubbles of radius a are passing at a volumetric flow rate of Q_a mL/sec. We let V_l be the volume of liquid being treated. The number of bubbles passed through the column per second is then given by

$$N = Q_a \Big/ \frac{4\pi a^3}{3} \tag{60}$$

If we let $c(t)$ be the number of floc particles per milliliter at time t, then

$$-V_l\,dc = c3\pi\delta ah\,\frac{3Q_a}{4\pi a^3}\,dt \tag{61}$$

gives the rate of change of c with t for bubbles large enough to be in the inviscid regime. Integration of Eq. (61) yields

$$c(t) = c(0)\exp\left[\frac{-9Q_a\delta ht}{4a^2V_l}\right] \tag{62}$$

In similar fashion we find that

$$c(t) = c(0)\exp\left[\frac{-9Q_a\delta^2 ht}{4a^3V_l}\right] \tag{63}$$

for the creeping flow regime.

Let us next consider a continuous-flow pool-type flotation apparatus of the sort diagrammed in Fig. 10. We let

Q_l = volumetric flow rate of liquid
Q_a = volumetric flow rate of air
c_0 = influent floc concentration
c_e = effluent floc concentration

The other symbols are as previously defined. In the steady state we have

$$c_0Q_l = c_eQ_l + c_e\,\frac{9\pi\delta ahQ_a}{4\pi a^3} \tag{64}$$

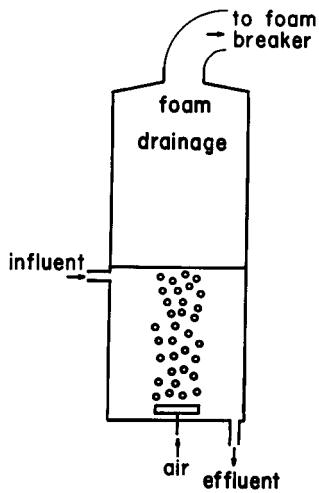

FIG. 10. A continuous-flow pool-type flotation apparatus.

if we assume that the pool is well-stirred during the detention time of the liquid but that this mixing is not sufficiently violent to seriously interfere with the movement of the bubbles. Equation (64) is solved for c_e to give

$$c_e = \frac{c_0}{1 + \dfrac{9\delta h Q_a}{4a^2 Q_l}} \tag{65}$$

Our analyses so far presume that all particle–bubble encounters ($r_{\min} \leq a + \delta$) lead to attachment. If the solids concentration or the depth of the pool, h, is large, the surface of the bubble may become saturated with solid before the bubble reaches the top of the pool, in which case it will be unable to attach additional particles. We assume that the bubbles are small enough so that the entire surface may be coated with solid, and examine the effects of this. We let b be the effective radius of a floc particle (assumed spherical), and we assume that $b \ll a$, the bubble radius. Then the maximum number of floc particles which a bubble can carry is given by

$$n_{\max} = \frac{4\pi a^2}{\pi b^2} = \frac{4a^2}{b^2} \tag{66}$$

Our previous analysis (the inviscid case) gave us $3\pi\delta ach$ as the number of particles captured by one bubble. Evidently for our previous analysis to be valid we must have

$$3\pi\delta ach \leq 4a^2/b^2 \tag{67}$$

which gives

$$ch \leq 4a/3\pi\delta b^2 \tag{68}$$

as the criterion which must be satisfied for our earlier formula, Eq. (62), to be valid.

If

$$ch > 4a/3\pi\delta b^2 \tag{69}$$

a bubble removes $4a^2/b^2$ particles. If the air flow rate is Q_a and the bubbles are of radius a, then the number of particles being removed per second is given by

$$\frac{4a^2}{b^2} \frac{Q_a}{\frac{4}{3}\pi a^3} = \frac{3Q_a}{\pi a b^2} \tag{70}$$

So for a concentrated slurry satisfying Eq. (69) we have

$$-V_l \frac{dc}{dt} = \frac{3Q_a}{\pi a b^2} \tag{71}$$

which integrates to give

$$c(t) = c_0 - \frac{3Q_a t}{\pi a b^2 V_l}, \qquad 0 \le t \le t' \tag{72}$$

where t' is determined as follows. From Eq. (69) we have

$$c(t') = \frac{4a}{3\pi\delta b^2 h} \tag{73}$$

so that

$$c_0 - \frac{3Q_a t'}{\pi a b^2 V_l} = \frac{4a}{3\pi\delta b^2 h} \tag{74}$$

and

$$t' = \left(c_0 - \frac{4a}{3\pi\delta b^2 h}\right)\frac{\pi a b^2 V_l}{3Q_a} \tag{75}$$

For $t > t'$ the analysis leading to Eq. (62) is valid, which yields

$$c(t) = \frac{4a}{3\pi\delta b^2 h} \exp\left[\frac{-9Q_a\delta h(t-t')}{4a^2 V_l}\right], \qquad t > t' \tag{76}$$

where we use Eq. (73) to fit $c(t)$ at t'. We note that dc/dt is continuous at t', which it should be on physical grounds.

For a continuous-flow pool-type apparatus, if

$$c_e > 4a/3\pi\delta b^2 h \tag{77}$$

the bubbles are saturated with floc, and we have

$$c_0 Q_l = c_e Q_l + \frac{3Q_a}{\pi a b^2} \tag{78}$$

on using Eq. (71) to determine the rate of particle removal in the foam. This yields

$$c_e = c_0 - \frac{3Q_a}{\pi a b^2 Q_l} \tag{79}$$

for concentrated slurries satisfying Eq. (77).

Conclusions

Our analysis indicates that the bubbles used in foam flotation from liquid pools should be large enough so that their movement is well out of the creeping flow regime; we recall, however, that viscous drag forces may strip floc particles off of bubbles which are too large (*19*). The rate of

removal of particles is first order and is proportional to air flow rate, depth of pool, and range of the bubble–floc particle interaction potential. It is inversely proportional to the square of the bubble radius and to the volume of liquid being treated. These conclusions apply to bubbles in the inviscid flow regime. Bubbles in the creeping flow regime are much less effective. Removal efficiencies from continuous-flow pool reactors exhibit similar characteristics. We note that concentrated slurries, which satisfy Eq. (69), exhibit removal rates which are independent of floc concentration, pool depth, and range of interaction potential.

Acknowledgments

This work was supported by the U.S. Environmental Protection Agency and the Vanderbilt University Research Council.

REFERENCES

1. R. Lemlich (ed.), *Adsorptive Bubble Separation Techniques*, Academic, New York, 1972.
2. P. Somasundaran, *Sep. Sci.*, *10*, 93 (1975).
3. R. B. Grieves, *Chem. Eng., J.*, *9*, 3 (1975).
4. A. N. Clarke and D. J. Wilson, *Sep. Purif. Methods*, *7*, 55 (1978).
5. D. Bhattacharyya, J. A. Carlton, and R. B. Grieves, *AIChE J.*, *17*, 419 (1971).
6. R. B. Grieves, R. M. Schwartz, and D. Bhattacharyya, *Sep. Sci.*, *10*, 777 (1975).
7. D. Voyce and H. Zeitlin, *Anal. Chim. Acta*, *69*, 27 (1974).
8. F. Chaine and H. Zeitlin, *Sep. Sci.*, *9*, 1 (1974).
9. N. Rothstein and H. Zeitlin, *Anal. Lett.*, *9*, 461 (1976).
10. M. Hagadone and H. Zeitlin, *Anal. Chim. Acta*, *86*, 289 (1976).
11. D. J. Wilson, *Foam Flotation Treatment of Heavy Metals and Fluoride-Bearing Industrial Wastewaters*, Environmental Protection Technology Series, EPA-600/2-77-072, April 1977.
12. D. J. Wilson and E. L. Thackston, *Foam Flotation Treatment of Industrial Wastewaters, Laboratory and Pilot Scale*, Environmental Protection Technology Series, EPA-600/2-80-138.
13. T. E. Chatman, S.-D. Huang, and D. J. Wilson, *Sep. Sci.*, *12*, 461 (1977).
14. A. N. Clarke, B. L. Currin, and D. J. Wilson, *Sep. Sci. Technol.*, *14*, 141 (1979).
15. B. L. Currin, R. M. Kennedy, A. N. Clarke, and D. J. Wilson, *Ibid.*, *14*, 669 (1979).
16. D. J. Wilson, *Sep. Sci.*, *12*, 231 (1977).
17. D. J. Wilson, *Ibid.*, *12*, 447 (1977).
18. B. L. Currin, F. J. Potter, D. J. Wilson, and R. H. French, *Sep. Sci. Technol.*, *13*, 285 (1978).
19. J. E. Kiefer and D. J. Wilson, *Ibid.*, *15*, 57 (1980).
20. S.-D. Huang and W.-H. Lee, *Ibid.*, *14*, 689 (1979).
21. S.-D. Huang and D. J. Wilson, *Sep. Sci.*, *10*, 407 (1975).
22. E. J. W. Verwey and J. Th. G. Overbeek, *Theory of the Stability of Lyophobic Colloids*, Elsevier, Amsterdam, 1948.
23. D. J. Wilson, *Sep. Sci.*, *11*, 391 (1976).
24. D. F. Devereux and P. L. deBruyn, *Interaction of Plane-Parallel Double Layers*,

MIT Press, Cambridge, Massachusetts, 1963.
25. A. Ralston, in *Mathematical Methods for Digital Computers* (A. Ralston and H. S. Wilf, eds.), Wiley, New York, 1960.
26. G. M. Fair, J. C. Geyer, and D. A. Okun, *Water and Wastewater Engineering, Vol. II. Wastewater Treatment and Disposal*, Wiley, New York, 1968, Section 25-2.
27. A. M. Gaudin, *Flotation*, 2nd ed., McGraw-Hill, New York, 1956, pp. 340–355.
28. G. K. Batchelor, *Introduction to Fluid Mechanics*, Cambridge University Press, 1967.

Received by editor November 30, 1979